Hydrodynamic Force of Resistance of Tourist Underwater Vehicle's Bare Hull with Different Heads using OpenFOAM

Hidrodinamička sila otpora trupa turističke podmornice s različitim krajevima uz uporabu OpenFOAM-a

Hassan Saghi
University of Zagreb, Faculty of Mechanical Engineering and Naval Architecture, Croatia
Hakim Sabzevari University, Department of Civil Engineering, Sabzevar, Iran
E-mail: hasansaghi1975@gmail.com

Joško Parunov*
University of Zagreb
Faculty of Mechanical Engineering and Naval Architecture
Croatia
E-mail: Josko.Parunov@fsb.hr

DOI 10.17818/NM/2023/1.3
UDK 629.58:338.48
551.465.11
Original scientific paper / *Izvorni znanstveni rad*
Paper received / *Rukopis primljen:* 14. 6. 2022.
Paper accepted / *Rukopis prihvaćen:* 16. 12. 2022.

Abstract

Power reduction is the central goal to maximize cruising duration of tourist underwater vehicles (UV) that can be achieved by shaping the hull. So, in this paper, hydrodynamic force of resistance of the tourist UV's bare hull is analysed. A numerical model based on Computational Fluid Dynamics in OpenFOAM is developed to simulate the longitudinal movement of an UV in a viscous and incompressible fluid for the infinite water depth. Three head geometries, including both spherical heads (S-S), spherical bow and elliptical stern head (S-E), and UV with both elliptical heads (E-E) are compared. At the first step, the effects of the length-to-diameter ratio and forward speed is studied for the S-S UV. The mesh size is calibrated using Grid Convergence Index, provided by ASME, while the model validation is based on the results for cube and sphere as well as by comparison with resistance coefficient of a SUBOFF bare hull. S-E and E-E UVs are then analysed for typical length-to-diameter ratio, comparing their force of resistance to the S-S type. The elongated elliptical heads are in many cases found favourable compared to the spherical heads. The results of this study may be useful for the conceptual design of tourist UV and for verification of the complex numerical models that are necessary to account for the influence of appendages on the force of resistance of such innovative UV.

KEY WORDS

tourist underwater vehicle
bare hull
spherical head
elliptical head
force of resistance
OpenFOAM
Computational Fluid Dynamics

Sažetak

Redukcija potrebne snage poriva glavni je cilj za maksimiziranje trajanja putovanja turističkih podmornica, što se može postići pažljivim oblikovanjem trupa. U ovome radu analizira se hidrodinamička sila otpora trupa turističke podmornice bez privjesaka i dodatne vanjske strukture. Razvijen je numerički model koji se temelji na računalnoj dinamici fluida (CFD) u OpenFOAM-u da bi se simuliralo uzdužno kretanje podmornice kroz viskozan i nestlačiv fluid u vodi neograničene dubine. Uspoređuju se tri geometrije krajeva podmornice, uključujući oba sferna kraja (S-S), sferni pramac i eliptičnu krmu (S-E), te podmornicu s oba eliptična kraja (E-E). Kao prvi korak analiziraju se učinci omjera duljine i promjera i brzine napredovanja za S-S tip. Kalibrirana je veličina mreže s pomoću Grid Convergence indeksa, koji propisuje ASME, dok se provjera valjanosti modela temelji na rezultatima za kocku i sferu te usporedbi s koeficijentom otpora SUBOFF trupa. Zatim se, za tipičan omjer duljine i promjera analiziraju S-E i E-E tipovi podmornice, uspoređujući njihovu silu otpora sa S-S tipom. Produljeni eliptični krajevi podmornice su se u većini slučajeva pokazali povoljnijim rješenjem u usporedbi sa sfernim krajevima. Rezultati ovoga istraživanja mogli bi se upotrijebiti za konceptualno projektiranje turističke podmornice, kao i za provjeru valjanosti složenih numeričkih modela koji su neophodni da bi se objasnio utjecaj privjesaka i dodatne vanjske strukture na silu otpora podmornice.

KLJUČNE RIJEČI

turistička podmornica
trup
sferni kraj čvrstog trupa
eliptični kraj čvrstog trupa
sila otpora
OpenFOAM
računalna dinamika fluida

1. INTRODUCTION / *Uvod*

In design of the naval submarines, the primary concern is usually their acoustic signature [1-3]. For a tourist underwater vehicle (UV), however, the central objective becomes power requirement to maximize cruising duration. Power reduction can be achieved by adopting energy-saving propulsion systems, controlling the boundary layer on the surface of the UV, and shaping the hull. Hydrodynamic shaping is therefore an important part of submarines and other UVs design.

Optimization of the bare hull form of submarine was presented in [4], while DREA (Defense Research Establishment Atlantic) model, as one of the standard bare submarine hull forms is proposed [5-6]. DREA model specifies the bare hull in three parts: bow, mid-body, and tail. In the initial design, the envelope consists of a pure tear drop shape, with the forward body making up 40% of its length and the after body making up 60% [7]. The bare hull geometry to find the optimum shapes for the nose and tail of an Autonomous Underwater Vehicle (AUV) was studied by Divsalar [8]. That study involved calculation of the hydrodynamic coefficients of a SUBOFF model developed by DARPA (Defense Advanced Research Projects Agency) with different length-to-diameter ratios, tail shapes, and sailing

* Corresponding author

speeds. DARPA developed the SUBOFF project to evaluate different flow field predictions for an axisymmetric hull, with and without appendages [9]. Accordingly, hull shapes with bullet noses and sharp tails with length-to-diameter ratio equal to 7.14 had the best performance.

Equations were defined for the optimal design of submarines. For instance, Myring's hull profile equations were developed to reduce underwater force of resistance when designing the hull shape of hybrid underwater gliders [10], while these equations are then used in practical design [11]. Autonomous and unmanned UVs are often designed using equations presented in Groves et al. [12]. Joung et al. [13] developed a CFD model to optimize the AUV's profile based on minimum force of resistance, using Myring's equations, while De Barros et al. [14] experimentally studied the submerged bodies designed by the same relationships. Saghi et al. [15] suggested equations based on Artificial Neural Network (ANN) to estimate the resistance coefficient of a submarine with spherical heads, variable length-to diameter ratio, and for different forward and transverse speeds.

Other studies emphasized the optimization of the submarine's appendages, such as the rudder and tail, to minimize its force of resistance. An example is the tail cone angle, which is one of the major parameters of a submarine's geometrical design. The tail cone angle of the DARPA Suboff AFF8 UV was studied by Ozden et al. [16]. A modification of the depth rudder system by Kiciński and Jurczak [17] was used to investigate the force of resistance characteristics of submarines. This was done by modelling two kinds of rudder geometry: parallel and X-type.

There has been much discussion about the effect of surface roughness caused by several reasons such as welding seams, coatings, or biofouling on the force of resistance characteristics of submarines. In a study conducted by Uzun et al. [18], the impact of barnacle type biofouling roughness on submarine performance is examined. The effects of antifouling coating system, with a range of roughness and fouling conditions, on the force of resistance and powering characteristics were evaluated by Schultz [19].

A submarine operation in different environments such as submerged and free surface conditions (including calm and wave conditions) has been investigated. The added force of resistance of submarines due to deck wetness at surface conditions was studied by Moonesun et al. [20]. They determined deck flooding of submarines caused by the wave making pattern at the bow. Similarly, Dong et al. [21] simulated a submarine sailing near the surface with long-crested waves. They found that irregular waves cause fluctuations in the hydrodynamic force exerted on the submarine, even below the surface. The effect of the water depth, including free surface conditions were studied by Gatin et al. [22], where the effect of the external structures was also discussed.

As mentioned earlier, submarines and other UVs designs should incorporate hydrodynamic shaping, and some research has been conducted on optimizing submarine bare hull forms [4-9]. In this regard, , the purpose of this paper is to present Computational Fluid Dynamics (CFD) analysis of UV's bare hull geometry with spherical heads (*S-S*), spherical bow and elliptical stern (*S-E*), and both elliptical heads (*E-E*) (see Figure 1), with respect to the forward speed in the infinitely deep water. The open-source CFD software OpenFOAM is used for that purpose. Other options of head's geometries are also possible, i.e., partially conical head with spherical dome or tory-spherical head, but not considered herein. The present study is inspired by a tourist UV with acrylic cylindrical hull, designed to provide visitors a view of the surrounding ocean in a comfortable manner [23]. The overall length of the studied UV is about 25 m, while the external diameter of the acrylic hull reads 2.64 m. The designed diving depth is 50 meters, and the maximum forward speed is 2.5 knots. The hull of the UV has spherical heads on both ends. The studied UV can accommodate 48 passengers and 2 crew members. The geometry variation in the present study is limited to the variation of geometry of the UV's steel heads since the central part consists of the acrylic cylinders and its shape is therefore fixed. Length-to-diameter ratio of the bare hull is also varied to observe its impact on the force of resistance while keeping the internal volume constant. The present study deals with the bare hull of the UV while the complete design consists also of external structures [22], which increases the hydrodynamic force of resistance. Such considerations are beyond the scope of the study while the present results may be used in the conceptual design and for verification of the complex numerical calculations of the hull with appendages.

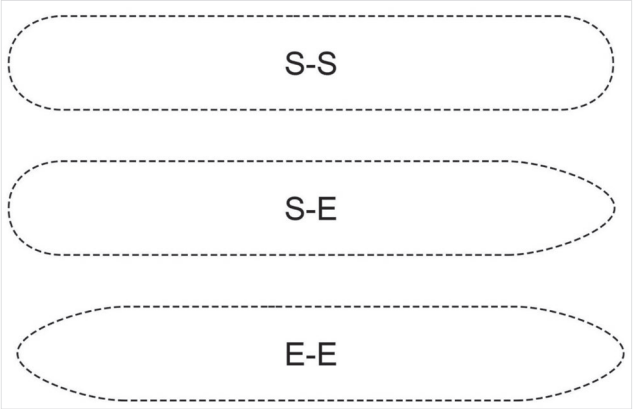

Figure 1 A schematic sketch showing three types of UV hulls (S-S, S-E, E-E).

Slika 1. Shema triju tipova trupa (S-S, S-E, E-E)

2. METHODOLOGY / *Metodologija*

In the present study, a submerged bare hull of a UV was modelled in a viscous and incompressible fluid so that the fluid flow was considered turbulent. Accordingly, Reynolds Averaged Navier Stokes (RANS) equations are used as the governing equations [24-27]:

$$div\left(\rho\underline{V}\right) = 0 \tag{1}$$

$$\frac{\partial}{\partial t}\left[\rho\underline{V}\right] + div\left[\rho\underline{V}\underline{V}\right] = -\nabla\underline{p} + div\left[\underline{\tau} - \rho\underline{V'V'}\right] + \underline{f_b} \tag{2}$$

The nomenclature is presented at the end of the paper.

To solve the RANS equations, the Pressure Implicit Method with Pressure Linked Equations (*PIMPLE*) algorithm was developed, and the pimpleFOAM solver was used. Different terms of the discretized equations, such as derivative terms, gradient parameters, Laplace derivative terms, and divergence terms, were discretized using 1st order implicit Euler, 2nd order centre Gauss linear, skewness corrected centre Gauss linear correction, and Upwind schemes, respectively [28]. By using

block mesh and refinement techniques, a cylindrical domain and a Cartesian structured grid were generated. Different boundary conditions summarized in Table 1 were used for the velocity, pressure, kinetic energy, and dissipate rate on the boundaries shown in Figure 2.

Parametric equations for the spherical and elliptical bow and stern read:

$$\frac{x^2}{(0.5D_s)^2}+\frac{y^2}{(0.5D_s)^2}+\frac{z^2}{(0.5D_s)^2}=1 \quad \text{for spherical bow and stern} \quad (3)$$

$$\frac{x^2}{R_b{}^2}+\frac{y^2}{(0.5D_s)^2}+\frac{z^2}{(0.5D_s)^2}=1 \quad \text{for elliptical bow} \quad (4)$$

$$\frac{x^2}{R_s{}^2}+\frac{y^2}{(0.5D_s)^2}+\frac{z^2}{(0.5D_s)^2}=1 \quad \text{for elliptical stern} \quad (5)$$

To satisfy the symmetry boundary condition for around the domain, the domain length (L_t) and diameter (D_t) were considered as L_t=1.4L_{oa} and D_t=4D_s, respectively [29].

In addition, the *K-Epsilon* two-equation model was used to account for turbulence [30-31].

$$\frac{\partial}{\partial t}[\rho k]+div[\rho V k]=div\left[\mu_{eff,k}\nabla k\right]+P_k-\beta\rho k\varepsilon \quad (6)$$

$$\frac{\partial}{\partial t}[\rho \varepsilon]+div[\rho V \varepsilon]=div\left[\mu_{eff,\varepsilon}\nabla \varepsilon\right]+C\varepsilon_1\frac{\varepsilon}{k}P_k-C_{\epsilon 2}\rho\frac{\varepsilon^2}{k} \quad (7)$$

where $C_{\varepsilon 1}=1.44 C_{\varepsilon 2}=1.92 \beta=0.09$ $\mu_{eff,k}=\mu+\frac{\mu_t}{\sigma_k}$ $\mu_{eff,\varepsilon}=\mu+\frac{\mu_t}{\sigma_\varepsilon}\sigma_k=1.0\sigma_\omega=1.3.$

To estimate pressure force of resistance and friction force of resistances along *x* axis, dynamic pressure and shear stress are integrated over the surface of the body as follows:

$$R_P=\int_S pn_x dA \quad (8)$$

$$R_f=\int_S \tau_{xy}n_y dA+\int_S \tau_{xz}n_z dA \quad (9)$$

Total force of resistance is calculated as follows:

$$R=R_P+R_f \quad (10)$$

The resistance coefficient reads:

$$C_R=\frac{R}{\frac{1}{2}\rho S V_f^2} \quad (11)$$

where *S* is the surface area of the UV's bare hull.

3. MESH SIZE CALIBRATION / *Kalibracija veličine mreže*

To determine the appropriate mesh size for the numerical model, a cube with edge length of L_c = 0.45 m was placed at a cylinder of 6 m length and 2 m diameter (see Figure 3(a)). The total force of resistance of the cube against the fluid flow is estimated by considering the input boundary condition as a constant velocity. The mesh size dependency was examined for a cube against a constant fluid flow with a velocity of 10 m/s. According to Figure 3(b), the total force of resistance was estimated at different mesh sizes (*ms*), and the numerical results showed that the uniform mesh sizes with *ms<0.03m* (*ms*/L_c < 0.067) did not significantly affect the total force of resistance.

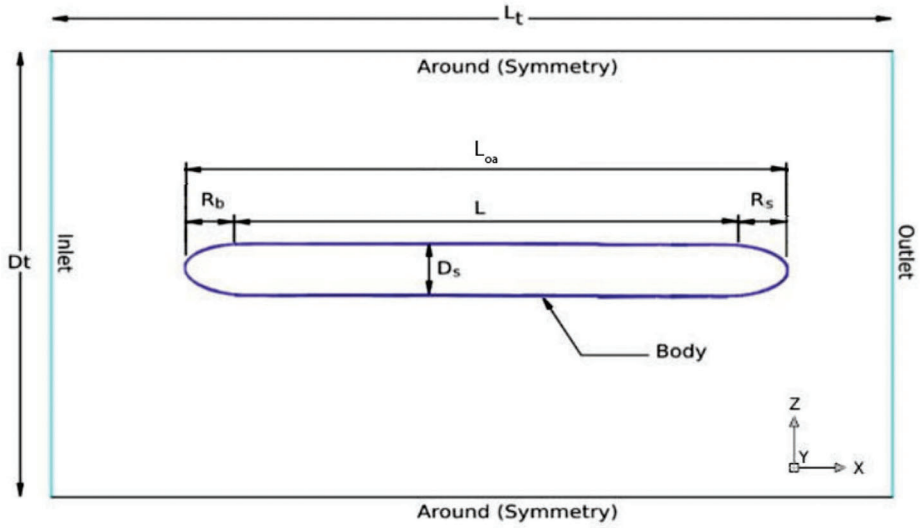

Figure 2 Schematic sketch of the UV geometry, domain, and boundary conditions. (*x* axis is oriented from the bow to the stern).
Slika 2. Shema geometrije podmornice, domene i rubnih uvjeta (x os pruža se od pramca prema krmi)

Table 1 Boundary conditions used for different parameters.
Tablica 1. Rubni uvjeti korišteni za različite parametre

Boundary	Velocity	Pressure	Kinetic energy (k)	Dissipation rate (ε)
Inlet	Fixed Value	Zero Gradient	Fixed Value	Fixed value
Outlet	Inlet Outlet	Fixed Value	Inlet Outlet	Inlet Outlet
Body	Moving wall velocity	Zero Gradient	Wall Function	Wall function
around	Symmetry	Symmetry	Symmetry	Symmetry

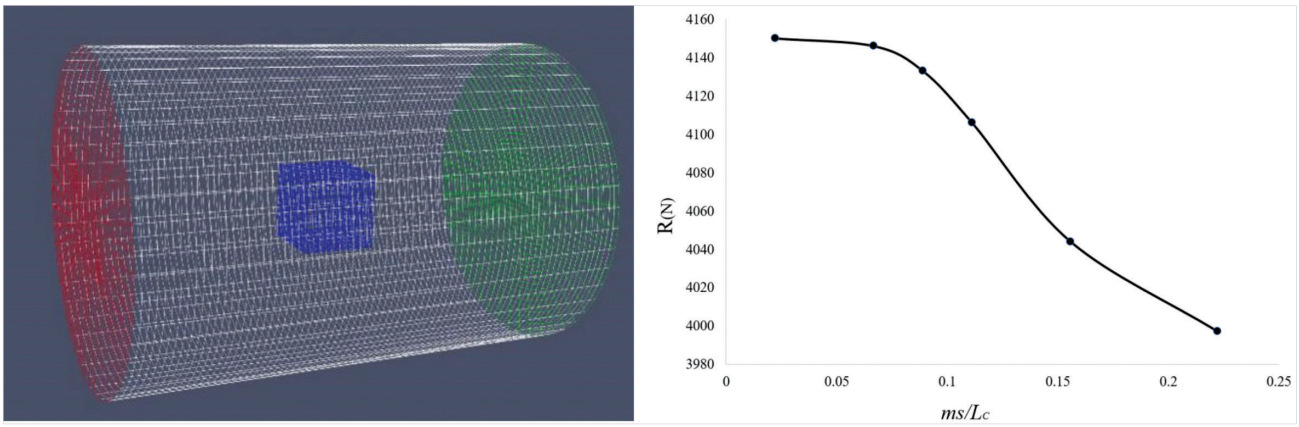

Figure 3 (a) The generated mesh of the cube inside a cylinder in OpenFOAM, (b) Mesh size dependence evaluation.
Slika 3. (a) Generirana mreža kocke u cilindru u OpenFOAM, (b) Ovisnost sile otpora o veličini mreže

The Grid Convergence Index (*GCI*) method, provided by ASME was used to evaluate the mesh size convergence. To do this, GCI_{fine}^{21} and GCI_{coarse}^{32} were estimated as follows [32]:

$$GCI_{fine}^{21} = \frac{1.25e_a^{21}}{r_{21}^p - 1} \tag{12}$$

$$GCI_{coarse}^{32} = \frac{1.25e_a^{32}}{r_{32}^p - 1} \tag{13}$$

where $r_{21} = \frac{ms_2}{ms_1}$, $r_{32} = \frac{ms_3}{ms_2}$, p is estimated by solving equations (14) to (16), and by using fixed-point iteration as:

$$p = \frac{1}{ln(r_{21})}\left|ln\left|\frac{\epsilon_{32}}{\epsilon_{21}}\right| + q(p)\right| \tag{14}$$

$$q(p) = ln\left(\frac{r_{21}^p - s}{r_{32}^p - s}\right) \tag{15}$$

$$s = 1 \cdot sgn\left(\frac{\epsilon_{32}}{\epsilon_{21}}\right) \tag{16}$$

and $\epsilon_{21} = \frac{R_2 - R_1}{R_1}$, $\epsilon_{32} = \frac{R_3 - R_2}{R_2}$, $e_a^{21} = \left|\frac{R_1 - R_2}{R_1}\right|$, $e_a^{32} = \left|\frac{R_2 - R_3}{R_2}\right|$.

The parameters ϵ_{21}, and ϵ_{32} are the relative error, which are also informative parameters. So, the parameters GCI_{fine}^{21}, GCI_{coarse}^{32}, ϵ_{21} and ϵ_{32} were estimated for four groups of meshes (fine, middle, and coarse) and outlined in Table 2.

Table 2 shows that in row 4, the ϵ_{21} and GCI_{fine}^{21} for *ms*=0.03m are much lower than the maximum acceptable value of 1%, which indicates that the mesh size is small enough for future computations. Accordingly, that mesh size is used to estimate the resistance coefficient of the cube against fluid flows with different Reynolds numbers $\left(R_e = \frac{\rho V_f L_c}{\mu}\right)$. The results are compared with

Table 2 Estimation of convergence parameters for different mesh sizes.
Tablica 2. Procjena parametara konvergencije za različite veličine mreže

	ms	*R*	ϵ_{21}(%)	ϵ_{32}(%)	GCI_{fine}^{21} (%)	GCI_{coarse}^{32}(%)
1	0.05,0.07,0.1	4106,4044,3977	-1.51	-1.65	4.557	3.272
2	0.04,0.05,0.07	4133,4106,4044	-0.653	-1.51	2.087	2.925
3	**0.03**,0.04,0.05	4146,4133,4106	-0.312	-0.653	0.186	0.580
4	0.01,**0.03**,0.04	4150,4146,4133	**-0.0964**	-0.312	**0.001**	0.122

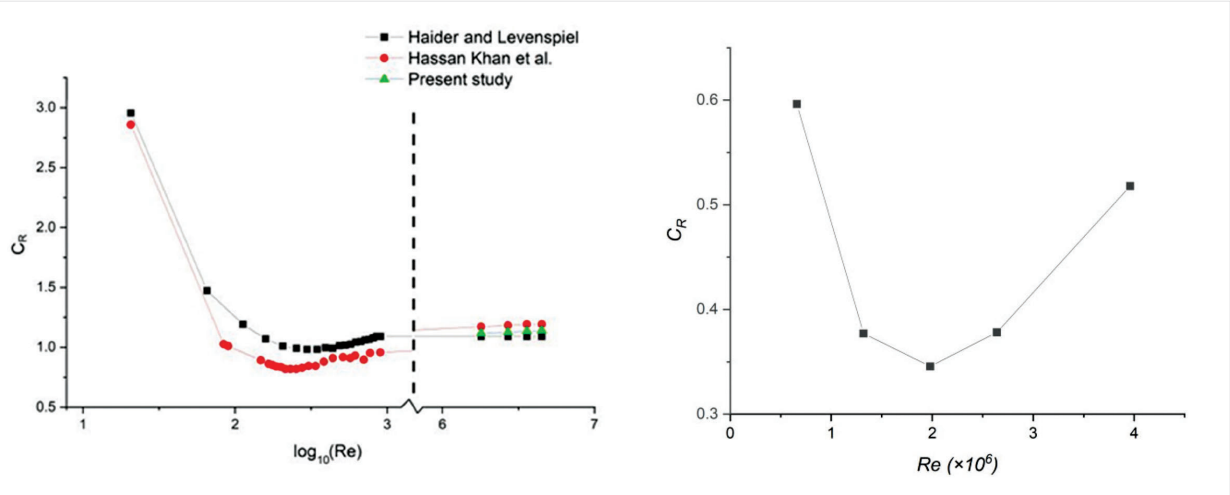

(a) (b)

Figure 4 The resistance coefficient of different geometries against fluid flowing at different Reynolds numbers (a) a cube of 0.45m length, (b) a sphere of 2.64 m diameter.
Slika 4. Koeficijent otpora različitih geometrija u odnosu na Reynoldsov broj (a) kocka duljine 0.45 m, (b) sfera promjera 2.64 m

Haider and Levenspiel [33] and Hassan Khan et al. [34] and shown in Figure 4-a. The results indicate a good agreement with the resistance coefficient calculated by other researchers.

In another test, the resistance coefficient of a sphere with the diameter of 2.64 m was estimated against fluid flows with different Reynolds numbers $\left(R_e = \frac{\rho V_f D_{SP}}{\mu}\right)$, as shown in Figure 4-b. The average drag coefficient of 0.45 was calculated for different Reynolds numbers. In the reference of Mikhailov et al. [35], the resistance coefficient of a sphere is estimated between 0.4 and 0.5 for Reynolds numbers greater than 10^4. Consequently, the average of 0.45 was found to be close to the amount suggested in Mikhailov et al. [35].

4. RESULTS / *Rezultati*

The main objective of the present study is the modelling of the bare hull of a UV against different forward speeds, to determine influence of the geometry on the hydrodynamic force of resistance. For that purpose, credible range of tourist UV geometries, represented by the ratio L/D_S is defined and shown in Table 3. In Table 3, L represents the length of the cylindrical hull, L_{oa} represents the overall length including the heads, and D_S represents the diameter of the cylindrical hull of the UV. The geometries are defined by keeping the total internal volume of the UV as constant.

Each of 9 geometry variations given in Table 3 was generated by using blockMesh, which is a utility in OpenFOAM for generating multiblock hexahedral meshes [28].

A total of 13 different forward speeds (0.25, 0.35, 0.5, 0.6, 0.7, 0.8, 0.9, 1.0, 1.1, 1.2, 1.3, 1.4 and 1.5 m/s) are analysed, covering range of speeds for which the studied UV is designed (0.5 knots to 2.5 knots). Therefore, a total of 117 cases listed in the Appendix are calculated.

As the geometry of the UV is different compared to the cube, the mesh convergence parameters *GCI* and ε are calculated for the forward speed 1 m/s of case 5 of the UV and shown in Table 4.

Table 3 The dimensions of the UV for different L/D_S ratios
Tablica 3. Dimenzije podmornice za različite L/D_S omjere

Case	$L(m)$	$L_{oa}(m)$	$D_S(m)$	L/D_S	$V_0(m3)$
1	25	27.44	2.44	10.2	124.50
2	24	26.49	2.49	9.6	124.95
3	23	25.54	2.54	9.1	125.12
4	22	24.59	2.59	8.5	125.00
5	21.06	23.7	2.64	8.0	124.91
6	20	22.7	2.7	7.4	124.81
7	19	21.76	2.76	6.9	124.68
8	18	20.83	2.83	6.4	125.09
9	17	19.9	2.9	5.9	125.05

From the last row in Table 4, it may be seen that GCI_{fine}^{21} and ϵ_{21} of *ms*=0.03 m are less than the limiting value of 1%, indicating that the mesh size 0.03 m is appropriate.

4.1. Hydrodynamic analysis of the bare hull of the UV with both spherical heads (S-S) / *Hidrodinamička analiza trupa podmornice s dva sferna kraja (S-S)*

A total of 117 different cases, as described in the previous section, are modelled, and analysed in OpenFOAM. In these cases, the radius of the bow and stern heads of the UV were considered as $R_b = R_S = \frac{D_S}{2}$ (see Fig. 2). The analysis is performed using supercomputer Isabella, based in SRCE – University of Zagreb Computing Centre. Isabella consists of 135 worker nodes, 3100 processor cores, 12 GPUs, and 756 TiB of data storage [36]. OpenFOAM computation for each of 117 cases lasted for about 18000 s, so the total running time was about 35100 min. Results of the analysis are presented in Figure 5, where hydrodynamic characteristics are presented against L/D_S and forward speed UV.

Table 4 Estimation of the mesh size dependency parameters of the case 5 of the UV for the forward speed 1m/s.
Tablica 4. Procjena parametara ovisnosti veličine mreže slučaja br. 5 podmornice za brzinu napredovanja od 1m/s

	ms	*R*	$\epsilon_{21}(\%)$	$\epsilon_{32}(\%)$	GCI_{fine}^{21} (%)	$GCI_{coarse}^{32}(\%)$
1	0.05,0.07,0.1	2235,2532,2720	13.29	7.42	17.54	9.04
2	0.04,0.05,0.07	1800,2235,2532	24.17	13.29	8.99	2.02
3	0.03,0.04,0.05	1771,1800,2235	1.64	24.17	0.06	2.12
4	0.01,**0.03**,0.04	1760,1771,1800	**0.62**	1.64	**0.01**	0.79

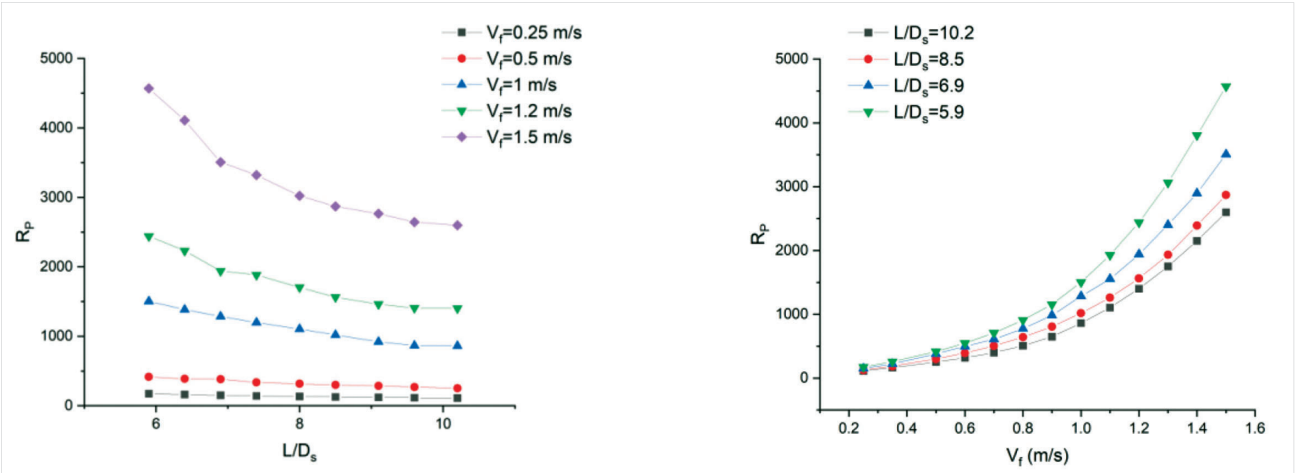

(a)

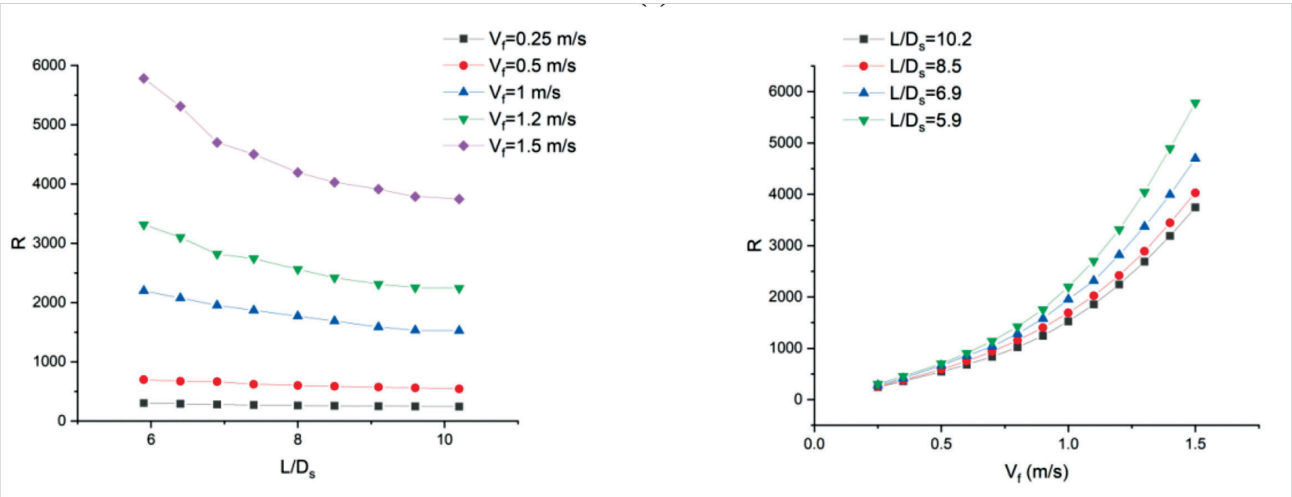

(b)

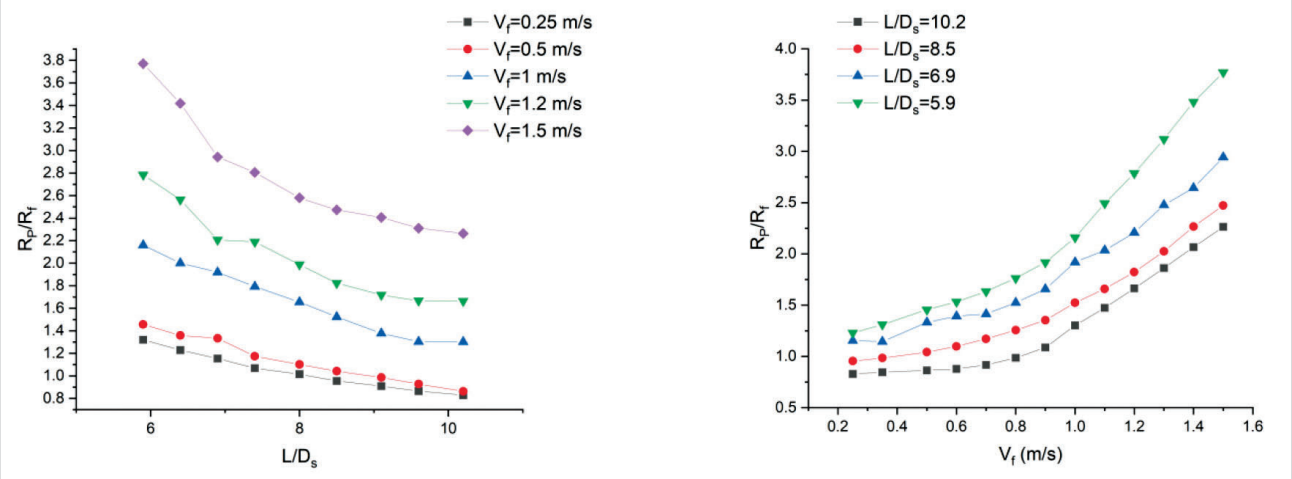

(c)

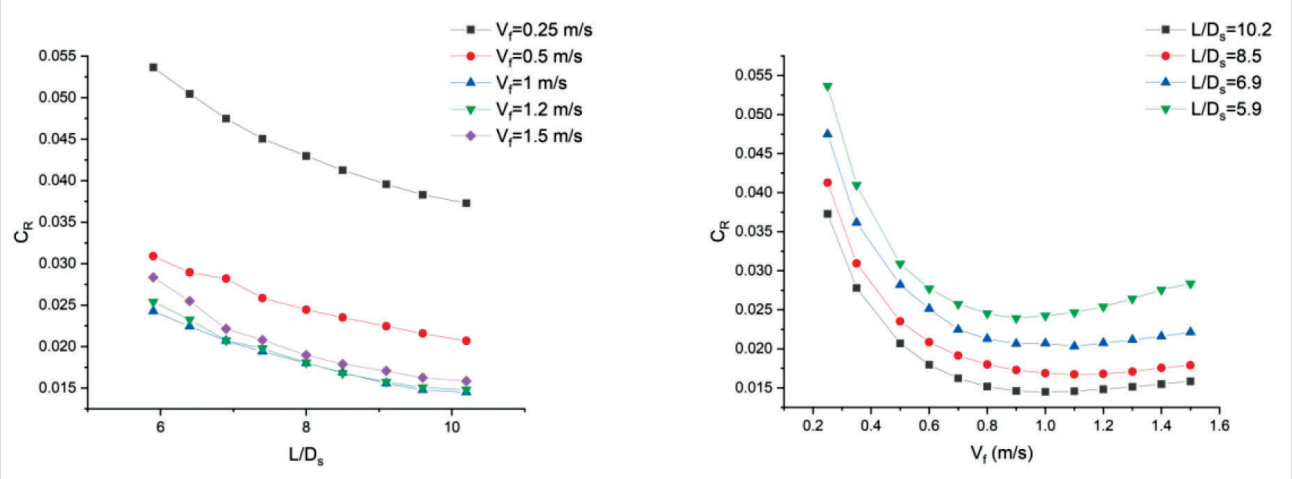

(d)

Figure 5 Variation of the hydrodynamic characteristics versus L/D_S (left) and forward speed (right), (a) Pressure force of resistance, R_P (b) Total force of resistance, R (c) Pressure force of resistance to friction force of resistance, R_P / R_f (d) Resistance coefficient, C_R.

Slika 5. Varijacija hidrodinamičkih karakteristika u odnosu na L/D_S (lijevo) i brzinu napredovanja (desno), (a) sila otpora tlaka, R_P (b) ukupna sila otpora, R (c) omjer sile otpora tlaka i sile otpora trenja, R_P/R_f, (d) koeficijent otpora, C_R

According to the results shown in Figure 5(a) and Figure 5(b), the pressure and total force of resistance of the UV has a direct and reverse relationship with V_f and L/D_S, respectively. Moreover, by increasing the forward speed, the L/D_S parameter's effectiveness on the pressure and total force of resistance is increased. As an example, the pressure force of resistance for V_f=0.25 m/s and for L/D_S =10.2 and 5.9 is 111 N and 173 N, respectively. Consequently, by decreasing the parameter L/D_S from 10.2 to 5.9, the pressure force of resistance is increased by 55%. In contrast, the increment of pressure force of resistance for V_f=1.5 m/s for the same amounts of L/D_S is around 76% (from 2599 N to 4571 N). In terms of total force of resistance, the effectiveness of the parameters L/D_S and V_f *is* less than those in comparison with the pressure force of resistance, so the total force of resistance is increased by around 24% and 54% by decreasing L/D_S from 10.2 to 5.9 and for V_f=0.35 m/s and 1.5m/s, respectively. Furthermore, the results show that the relationship between total force of resistance (*R*) and L/D_S is linear for low forward speeds. However, as the forward speed increases, the relationship becomes nonlinear. For all L/D_S, expectedly, the relationship between force of resistance and forward speed is nonlinear.

In Figure 5(c), it is evident that the pressure force of resistance is in most cases dominant over the friction force of resistance. It is always the case that R_p is larger than R_f for different L/D_S values and forward speeds greater than 0.9 m/s. For UVs with $L/D_S < 6.9$ and forward speeds less than 0.9 m/s, the pressure force of resistance is also larger than the friction force of resistance. The only cases when friction force of resistance exceeds pressure force of resistance, occur for the slender UVs ($L/D_S > 8$) and for the low forward speeds (V_f=0.6 m/s). As an example, the ratio of pressure force of resistance to friction force of resistance is 0.82 for V_f=0.25 m/s and L/D_S =10.2. In contrast, R_p/R_f is 3.77 for V_f=1.5 m/s and L/D_S =5.9.

The UV's resistance coefficient is shown in Figure 5(d). As forward speed increases, the resistance coefficients decrease so that maximum coefficients follow minimum forward speed (V_f =0.25 m/s). However, these coefficients are minimal for V_f =1.1 m/s, and they increase slightly for higher speeds.

It is interesting to compare results presented in Figure 5(d) with the results for the resistance coefficient of a SUBOFF bare hull, presented by Divsalar [8], where the resistance coefficient of the bare hull with bullet nose, sharp tail, for L_{oa}/D_S=7 and V_f=1.5 m/s reads around 0.02. On the other hand, the present results obtained for the resistance coefficient of the UV with spherical heads and L_{oa}/D_S = 7 reads around 0.023 (Figure 5(d)). So, we can claim that the results are consistent, even though the geometry of the SUBOFF bare hull is different from the geometry of the present UV. It should be noted that Divsalar [8] obtained excellent agreement of his CFD analysis with the experimental results.

4.2. Hydrodynamic analysis of the bare hull of the UV with spherical bow and elliptical stern head (S-E) / *Hidrodinamička analiza trupa podmornice sa sfernim pramcem i eliptičnom krmom (S-E)*

The bare hull of the UV *S-S* with L/D_S = 8 is used further as the representative case for the purpose of comparison with different head geometries. Thus, a UV *S-E* with L/D_S = 8, spherical bow with a radius of 1.32 and elliptical stern with changing longitudinal semi-axis R_s (see Figure 2) are modeled, and different scenarios are summarized in Table 5.

Based on scenarios summarized in Table 5, the total force of resistance of the UV is calculated, and the results are shown in Figure 6.

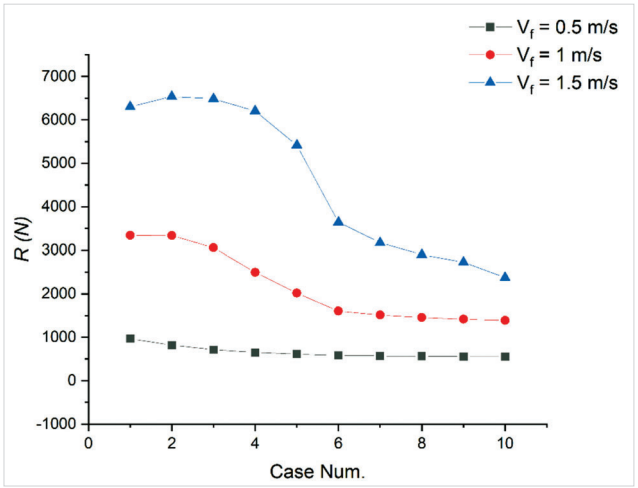

Figure 6 The variation of the total force of resistance of different UV cases S-E (see Table 5) and forward speeds (V_f) (L/D_S = 8).
Slika 6. Varijacija ukupne sile otpora različitih slučajeva podmornice tipa S-E (vidjeti Tablicu 5.) i brzina napredovanja (V_f) (L/D_S = 8)

Figure 6 shows that the bare hull of the UV *S-E* with R_S=2.07m (case 10 in Table 5) has the minimum force of resistance, so that the force of resistance of the UV in that case is reduced by around 38% compared to the UV *S-S* for V_f=1.5 m/s.

Table 5 Different scenarios of the UV S-E.
Tablica 5. Različiti scenariji za podmornicu tipa S-E

Case	1	2	3	4	5	6	7	8	9	10
L(m)	21.06	21.06	21.06	21.06	21.06	21.06	21.06	21.06	21.06	21.06
D_S(m)	2.64	2.64	2.64	2.64	2.64	2.64	2.64	2.64	2.64	2.64
R_b(m)	1.32	1.32	1.32	1.32	1.32	1.32	1.32	1.32	1.32	1.32
R_s(m)	0.57	0.72	0.87	1.02	1.17	1.47	1.62	1.77	1.92	2.07
R_s/R_b	0.43	0.55	0.66	0.77	0.89	1.11	1.23	1.34	1.45	1.57
$A(m^2)$	195.63	195.17	195.10	195.34	195.83	197.40	198.25	199.12	199.99	200.88

Table 6 Different scenarios of the UV E-E.
Tablica 6. Različiti scenariji za podmornicu tipa E-E

Case	1	2	3	4	5	6	7	8	9	10
$L(m)$	21.06	21.06	21.06	21.06	21.06	21.06	21.06	21.06	21.06	21.06
$D_s(m)$	2.64	2.64	2.64	2.64	2.64	2.64	2.64	2.64	2.64	2.64
$R_s(m)$	2.07	2.07	2.07	2.07	2.07	2.07	2.07	2.07	2.07	2.07
R_b(m)	0.57	0.72	0.87	1.02	1.17	1.47	1.62	1.77	1.92	2.07
R_b/R_s	0.43	0.55	0.66	0.77	0.89	1.11	1.23	1.34	1.45	1.57
$A(m^2)$	199.95	199.50	199.43	199.66	200.16	201.72	202.57	203.44	204.32	205.21

4.3. Hydrodynamic analysis of the bare hull of the UV with both elliptical heads (E-E) / *Hidrodinamička analiza trupa podmornice s dva eliptična kraja (E-E)*

In this step, UVs of the type *E-E* with elliptical bow with a longitudinal semi-axis R_b, and elliptical stern with a longitudinal semi-axis of 2.07 were modelled (see Figure 2 and Table 6), and the total force of resistance is shown in Figure 7 for V_f=0.5 m/s, 1 m/s, and 1.5 m/s.

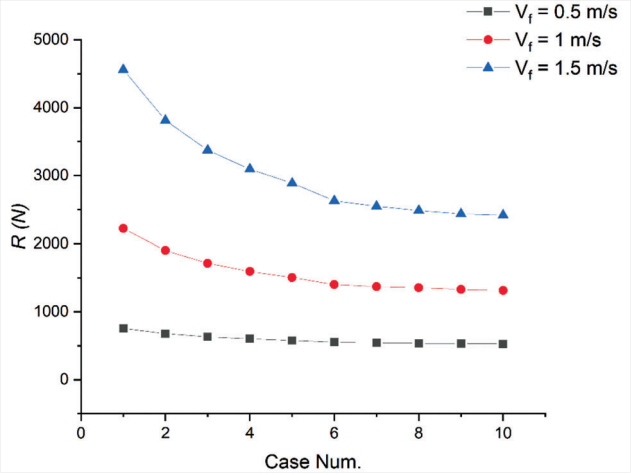

Figure 7 The variation of the total force of resistance of different UV cases E-E (see Table 4) and forward speeds (V_f) ($L/D_S = 8$).
Slika 7. Varijacije ukupne sile otpora različitih slučajeva podmornice tipa E-E (vidjeti Tablicu 4.) i brzina napredovanja (V_f) ($L/D_S = 8$)

Figure 7 illustrates that the force of resistance of the UV *E-E* is decreased as the longitudinal semi-axis of the ellipse R_b is increased. For instance, the UV's force of resistance for R_b=2.07 (case 10 in Table 6) and for V_f=1.5 m/s is 2417 N. For the same forward speed, the force of resistance of the spherical UV reads 4195 N. This means that the force of resistance of the UV *E-E* with R_b=2.07 is around 57% of the force of resistance of the spherical UV.

5. DISCUSSION / *Rasprava*

Here, we compare the total force of resistance of the selected bare hulls (case 5 in Table 3, case 10 in Table 5, and case 10 in Table 6) for different UV forward speeds. Figure 8 shows comparison of the force of resistance of *S-S*, *S-E*, and *E-E* geometries for different Reynolds numbers $R_e = \frac{\rho V_f L_{oa}}{\mu}$. The geometrical parameters of the selected *S-S*, *S-E*, and *E-E* UVs are provided in tables 3,4, and 5 respectively.

According to Figure 8, increasing the Reynolds number (forward speed) decreases the ratio of the force of resistance of the UV *E-E* to the UV *S-S*. For example, the force of resistance of the UV *E-E* (case 10 in Table 4) for R_e = 1.26×10^7 (V_f=0.5 m/s) is 527 N, which is about 87% of the force of resistance of the suggested

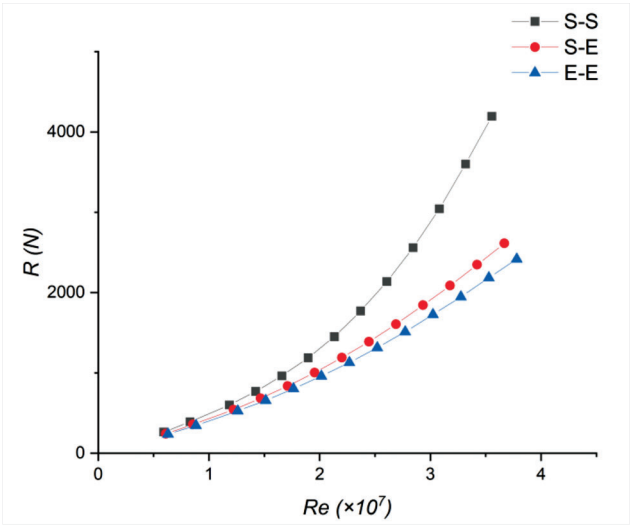

Figure 8 Comparison of the force of resistance of the UVs S-S (case 5), S-E (case 10), and E-E (case 10) for different Reynolds numbers.
Slika 8. Usporedba sile otpora podmornice tipa S-S (slučaj 5), S-E (slučaj 10) i E-E (slučaj 10) za različite Reynoldsove brojeve

UV *S-S* at the same forward speed (601 N). In contrast, the force of resistance of the UV *E-E* for R_e = 3.78 × 10^7 (V_f=1.5 m/s) (2417 N) is about 57% of that of the UV *S-S* (4195 N). Due to this, the efficiency of the geometry of the UV *E-E* increases as the UV forward speed increases as compared to the geometry of the UV *S-S*.

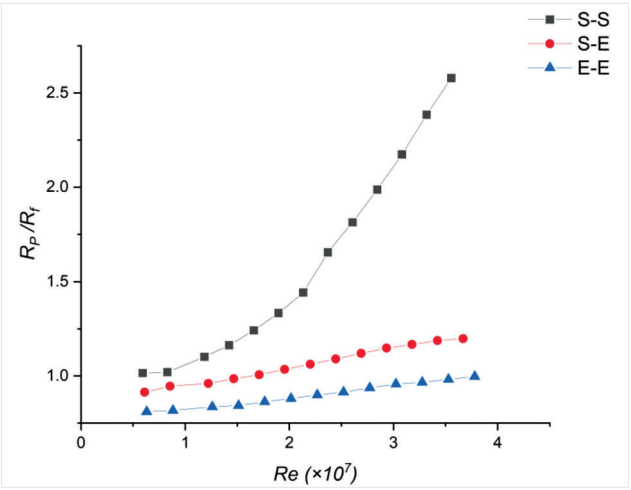

Figure 9 Comparison of the UV's pressure force of resistance to the friction force of resistance ratio of the UVs S-S (case 5), S-E (case 10), and E-E (case 10) for different Reynolds numbers.
Slika 9. Usporedba omjera sile otpora tlaka i trenja za podmornicu tipa S-S (slučaj 5), S-E (slučaj 10) i E-E (slučaj 10) za različite Reynoldsove brojeve

The pressure to friction force of resistance ratio for these UVs and for different Reynolds numbers are shown in Figure 9. The results show that the pressure to friction force of resistance ratio of the concept *E-E* is lower than that of the concept *S-S* so it reads approximately 1.0 for the UV *E-E* for $R_e = 3.78 \times 10^7$. However, the ratio is around 2.6 for the same Reynolds number for the UV *S-S*.

To clarify the effect of the geometry on the pressure distribution around the UVs' bare hull, Figure 10 shows the pressure distribution around the three types of UV heads (*S-S*, *S-E*, *E-E*), for the same forward speed (V_f =1.5 m/s). The results shown in Figure 10 indicate that the low-pressure area around the elliptical stern is reduced compared to the spherical stern, thereby reducing the force of resistance. Similarly, a reduction in the high-pressure area of the elliptical bow leads to a lower force of resistance.

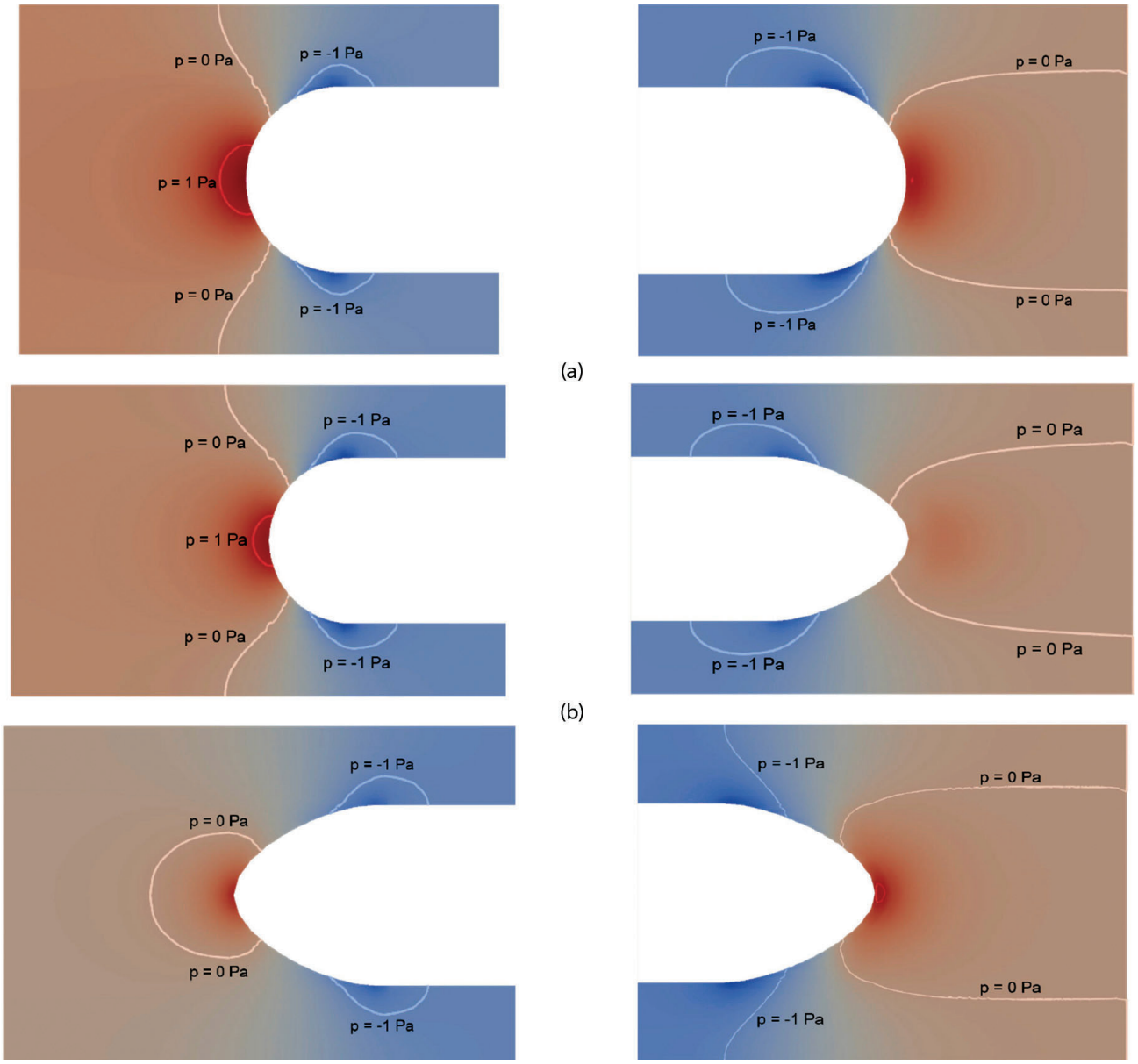

Figure 10 The pressure distribution around the bow and stern of the selected S-S, S-E, and E-E UV for V_f =1.5 m/s, (a) S-S, (b) S-E, (c) E-E.

Slika 10. Raspodjela tlaka oko pramca i krme odabranih S-S, S-E i E-E podmornica za V_f =1,5 m/s, (a) S-S, (b) S-E, (c) E-E

6. CONCLUSION / *Zaključak*

A Computational Fluid Dynamic numerical model in OpenFOAM is developed for the analysis of tourist underwater vehicle's (UV's) bare hull with different length-to-diameter aspect ratios and head geometries. To evaluate shape of the UV, hydrodynamic force of resistance is calculated. The mesh size is calibrated using Grid Convergence Index, provided by ASME, and employed on the case of the cube and UV. Model is validated based on the results of resistance coefficient for cube and sphere as well as by comparison with resistance coefficient of a SUBOFF bare hull with the same ratio of length to diameter (L_{od}/D_s). Based on the results of total of 177 cases analysed, the following conclusions may be drawn:

- total force of resistance of the UV has a direct and reverse relationship with V_f and L/D_s, respectively,
- the pressure force of resistance is in most cases dominant over the friction force of resistance,
- the results showed significant improvement of the hydrodynamic characteristics of the UV if the elongated elliptical heads are used instead of spherical heads, because of the reduction of the high- and low-pressure areas in the bow and stern regions respectively for the UV with elliptical heads. Thus,
  - the total hydrodynamic force of resistance of the UV with spherical bow and elliptical stern, and with L/D=8 is about 60-90 % of the corresponding case with both spherical heads,
  - the total force of resistance of the UV with both elliptical heads is about 55-85 % of the case with spherical heads.

The results are intended for the conceptual design of tourist UVs and for verification of complex numerical computations for UV's hull with external structure that significantly increases their hydrodynamic force of resistance.

Funding: The project is co-financed by the European Union from the European Regional Development Fund within the Operational Program "Competitiveness and Cohesion 2014-2020", project KK.01.2.1.02.0339 – Development of the multipurpose luxury touristic and research submarine.

Conflict of interest: None.

Acknowledgment / *Zahvala*

The project is co-financed by the European Union from the European Regional Development Fund within the Operational Program "Competitiveness and Cohesion 2014-2020", project KK.01.2.1.02.0339 – Development of the multipurpose luxury touristic and research submarine. The content of the publication is the sole responsibility of the project partner University of Zagreb, Faculty of Mechanical Engineering and Naval Architecture.

This research was performed using the resources of computer cluster Isabella based in SRCE – University of Zagreb University Computing Centre.

REFERENCES / *Literatura*

[1] Caresta, M., Kessissoglou & N. J. (2010). Acoustic signature of a submarine hull under harmonic excitation. *Applied Acoustics*, 71(1), 17-31. https://doi.org/10.1016/j.apacoust.2009.07.008

[2] Merz, S., Kinns R. & Kessissoglou, N. (2009). Structural and acoustic responses of a submarine hull due to propeller forces. *Journal of Sound and Vibration*, 325(1-2), 266-286. https://doi.org/10.1016/j.jsv.2009.03.011

[3] Jia, W., Chen, M., Xie, K. & Dong, W. (2022). Experimental and analytical investigations on vibro-acoustic characteristics of a submerged submarine hull coupled with multiple inner substructures. *Ocean Engineering*, 259, 111960. https://doi.org/10.1016/j.oceaneng.2022.111960

[4] Moonesun, M., Korol & Y. M. (2014). A review study on the bare hull form equations of submarine. The 16th Marine Industries Conference, Bandar Abbas, Iran, 1-9. https://www.sid.ir/paper/921039/en

[5] Baker, C. (2004). Estimating Drag Force on Submarine Hulls. Report DRDC Atlantic CR2004-125. Defence R & D Canada-Atlantic.

[6] Mackay, M. (2003). The Standard Submarine Model: A Survey of Static Hydrodynamic Experiments and Semi empirical Predictions, Technical report. Defence R & D Canada, Atlantic, TR 2003-079.

[7] Thornton Grant, B. (1994). A design tool for the evaluation of atmosphere independent propulsion in submarines. Massachusetts Institute of Technology. Master's thesis. https://www.hydrogen-peroxide.us/uses-oxygen-generation/US-Naval-Acad-Design-Tool-Air-Independent-Submarine-Propulsion-1979.pdf

[8] Divsalar, K. (2020). Improving the hydrodynamic performance of the SUBOFF bare hull model: a CFD approach. *Acta Mechanica Sinica*, 36, 44-56. https://doi.org/10.1007/s10409-019-00913-7

[9] Prestero, T. (1994). Verification of a Six-Degree of Freedom Simulation Model for the REMUS Autonomous Underwater Vehicle. Massachusetts Institute of Technology. Master's thesis. https://core.ac.uk/download/pdf/4429735.pdf

[10] Myring, D. F. (2016). *A Theoretical Study of Body Drag in Subcritical Axisymmetric Flow*. Published online by Cambridge University Press. https://doi.org/10.1017/S000192590000768X

[11] Ji, D. H., Choi, H. S., Kang, J. I., Cho, H. J., Joo, M. G. & Lee J. H. (2019). Design and control of hybrid underwater glider. *Advances in Mechanical Engineering,* 11(5), 1-9. https://doi.org/10.1177/1687814019848556

[12] Groves, N. C., Huang, T. T. & Chang, M. S. (1989). Geometric Characteristics of DARPA (Defense Advanced Research Projects Agency) SUBOFF Models (DTRC Model Numbers 5470 and 5471).

[13] Joung, T., Sammut K., He, F. & Lee, S. K. A (2009). A study on the Design Optimization of an AUV by Using Computational Fluid Dynamic Analysis. The Nineteenth International Offshore and Polar Engineering Conference. International Society of Offshore and Polar Engineers. Osaka, Japan. Paper Number: ISOPE-I-09-515.

[14] Barros, E. A., Pascoal, A. M. & Sá, E. D. (2006). Progress towards a method for predicting AUV derivatives. In: Proceedings of IFAC Manoeuvring Control Marine Crafts, 1-12.

[15] Saghi, H., Parunov, A. & Mikulic, A. (2022). Resistance Coefficient Estimation for a Submarine's Bare Hull Moving in Forward and Transverse Directions. *Applied Science*, 12, 10953. https://doi.org/10.3390/app122110953

[16] Ozden, Y. A., Ozden, M. C. & Celik, F. (2017). Numerical Investigation of Submarine Tail Form on the Hull Efficiency. Fifth International Symposium on Marine Propulsors, Espoo, Finland, June 2017. Corpus ID: 199557156.

[17] Kiciński, R. & Jurczak, W. (2021). Submarine Resistance Force Characteristics Determination After Modification of Depth Rudder System. *Advances in Science and Technology Research Journal*, 15(1), 1-9. https://doi.org/10.12913/22998624/125186

[18] Uzun, D., Sezen, S., Atlar, M. & Turan, O. (2021). Effect of biofouling roughness on the full-scale powering performance of a submarine. *Ocean Engineering,* Vol. 238, 109773. https://doi.org/10.1016/j.oceaneng.2021.109773

[19] Schultz, M. P. (2007). Effects of coating roughness and biofouling on ship resistance and powering. *Biofouling,* 23(5), 331-341. https://doi.org/10.1080/08927010701461974

[20] Moonesun, M., Javadi, M., Mousavizadegan, S. H., Dalayeli, H., Mikhailovich Korol Y. & Gharachahi, A. (2016). Computational fluid dynamics analysis on the added resistance of submarine due to Deck wetness at surface condition. *Proc IMechE Part M: J Engineering for the Maritime Environment*, 231(1), 128-136. https://doi.org/10.1177/1475090215626462

[21] Dong, K., Wang, X., Zhang, D., Liu, L. & Feng, D. (2022). CFD Research on the Hydrodynamic Performance of Submarine Sailing near the Free Surface with Long-Crested Waves. *Journal of Marine Science and Engineering*, 10(1), 1-29. https://doi.org/10.3390/jmse10010090

[22] Gatin, I., Čokić, J., Romić, D. & Parunov, J. (2022). CFD Study on the Influence of Exostructure Elements on the Resistance of a Submarine. *Journal of Marine Science and Engineering,* 10(10), 1542. https://doi.org/10.3390/jmse10101542

[23] Ćorak, M., Šperanda, Z., Čokić, J., Palaversa, M. & Parunov, J. (2023). Finite Element Simulations of Novel Submersible Design Based on the ASME Design-by-Analysis Approach. *Journal of Marine Science and Engineering,* 11(2), 275. https://doi.org/10.3390/jmse11020275

[24] Saghi, H. & Lakzian, E. (2017). Optimization of the rectangular storage tanks for the sloshing phenomena based on the entropy generation minimization. *Energy,* 128, 564-574. https://doi.org/10.1016/j.energy.2017.04.075

[25] Saghi, H., Mikkola, T. & Hirdaris, S. (2021). The influence of obliquely perforated dual baffles on sway induced tank sloshing dynamics. Proceedings of the Institution of Mechanical Engineers, *Part M: Journal of Engineering for the Maritime Environment,* 235(4), 905-920. https://doi.org/10.1177/1475090220961920

[26] Saghi, H., Ning, D. Z., Shunqi, P. & Saghi, R. (2022). Optimization of a dual-baffled rectangular tank against the sloshing phenomenon. *Journal of Marine Science and Application*, 21(1), 116-127. https://doi.org/10.1007/s11804-022-00257-y

[27] Saghi, R. & Saghi H. (2022). Numerical simulation of half-full cylindrical and bi-lobed storage tanks against the sloshing phenomenon. *Ocean Engineering,* 266, 112896. https://doi.org/10.1016/j.oceaneng.2022.112896

[28] OpenFOAM, The openFoam Foundation, User Guide. 10th July 2019. http://openfoam.org.

[29] Blazek, J. (2015). *Computational Fluid Dynamics, Principle and Applications.* 3rd ed. Butterworth-Heinemann. ISBN: 978-0-08-099995-1. https://doi.org/10.1016/C2013-0-19038-1

[30] Dean, R. G. & Dalrymple, R. A. (1991). *Water wave mechanics for engineers and scientists.* ISBN: 978-981-02-0420-4 (hardcover). https://doi.org/10.1142/1232

[31] Saghi, H., Mikkola T. & Hirdaris S. (2022). A machine learning method for the evaluation of hydrodynamic performance of floating breakwaters in waves. *Ships and Offshore Structures*, 17, 1447-1461. https://doi.org/10.1080/17445302.2021.1927358

[32] Celik, I. B., Ghia, U., Roache, P. J., Freitas, C. J., Coleman, H. & Raad, P. E. (2008). Procedure for Estimation and Reporting of Uncertainty Due to Discretization in CFD. *Journal of Fluids Engineering,* 130(7), 078001. https://doi.org/10.1115/1.2960953

[33] Haider, A. & Levenspiel, O. (1989). Drag coefficient and terminal velocity of spherical and nonspherical particles. *Powder Technology*, 58(1), 63-70. https://doi.org/10.1016/0032-5910(89)80008-7

[34] Hassan Khan, M., Sooraj, P., Sharma, A. & Agrawal, A. (2018). Flow around a Cube for Reynolds numbers between 500 and 55000. *Experimental thermal and fluid science,* 93, 257-271. https://doi.org/10.1016/j.expthermflusci.2017.12.013

[35] Mikhailov, M. D. & Silva Freire, A. P. (2013). The drag coefficient of a sphere: An approximation using Shanks transform. *Powder Technology*, 237, 432-435. https://doi.org/10.1016/j.powtec.2012.12.033

[36] University of Zagreb University Computing Centre (SRCE). https://www.srce.unizg.hr/en/isabella-cluster.

Nomenclature

Symbols

C_P	Pressure resistance coefficient
C_R	Resistance coefficient
D_s	Diameter of the submarine
D_{sp}	Diameter of the sphere
L	Length of the parallel middle body of submarine
L_C	Length of the cube
L_{oa}	Total length of submarine
V	Velocity vector
R	Resistance
R_b	Radius of the bow of the submarine
R_f	Friction resistance
R_p	Pressure resistance
R_S	Radius of the stern of the submarine
R_e	Reynolds number
S	Surface area of the submarine's bare hull
V	Velocity vector
V_f	Forward speed of the submarine
V_0	Volume of the submarine
$\underline{f_b}$	Body force
dx	Mesh size in x direction
dy	Mesh size in y direction
dz	Mesh size in z direction
n_x	Unit vector of the bare hull surface along the x axis
n_y	Unit vector of the bare hull surface along the y axis
ms	Mesh size
p	Dynamic pressure
t	Time
u	The velocity component in the direction x
v	The velocity component in the direction y
w	The velocity component in the direction Z
x	Direction x
y	Direction y
z	Direction Z
ε	Dissipation rate
τ_{xy}	Shear stress in the plane xy
τ_{xz}	Shear stress in the plane xz
μ	Dynamic viscosity
ρ	Fluid density
∇	Gradient operator

Abbreviations

AUV	Autonomous Underwater Vehicle
DARPA	Defense Advanced Research Projects Agency
DREA	Defense Research Establishment Atlantic
PIMPLE	Pressure Implicit Method with Pressure Linked Equations
RANS	Reynolds Average Navier Stokes
UV	Underwater Vehicle
VOF	Volume of Fluid

Appendix

Computational scenarios of the submarine with spherical heads at different speeds.

Case	$L(m)$	$L_{oa}(m)$	$D_S(m)$	L/D_s	$V_f(m/s)$
1	25	27.44	2.44	10.2	0.25
2	24	26.49	2.49	9.6	0.25
3	23	25.54	2.54	9.1	0.25
4	22	24.59	2.59	8.5	0.25
5	21.06	23.7	2.64	8.0	0.25
6	20	22.7	2.7	7.4	0.25
7	19	21.76	2.76	6.9	0.25
8	18	20.83	2.83	6.4	0.25
9	17	19.9	2.9	5.9	0.25
10	25	27.44	2.44	10.2	0.35
11	24	26.49	2.49	9.6	0.35
12	23	25.54	2.54	9.1	0.35
13	22	24.59	2.59	8.5	0.35
14	21.06	23.7	2.64	8.0	0.35
15	20	22.7	2.7	7.4	0.35
16	19	21.76	2.76	6.9	0.35
17	18	20.83	2.83	6.4	0.35
18	17	19.9	2.9	5.9	0.35
19	25	27.44	2.44	10.2	0.5
20	24	26.49	2.49	9.6	0.5
21	23	25.54	2.54	9.1	0.5
22	22	24.59	2.59	8.5	0.5
23	21.06	23.7	2.64	8.0	0.5
24	20	22.7	2.7	7.4	0.5
25	19	21.76	2.76	6.9	0.5
26	18	20.83	2.83	6.4	0.5
27	17	19.9	2.9	5.9	0.5
28	25	27.44	2.44	10.2	0.6
29	24	26.49	2.49	9.6	0.6
30	23	25.54	2.54	9.1	0.6
31	22	24.59	2.59	8.5	0.6
32	21.06	23.7	2.64	8.0	0.6
33	20	22.7	2.7	7.4	0.6
34	19	21.76	2.76	6.9	0.6
35	18	20.83	2.83	6.4	0.6
36	17	19.9	2.9	5.9	0.6

37	25	27.44	2.44	10.2	0.7
38	24	26.49	2.49	9.6	0.7
39	23	25.54	2.54	9.1	0.7
40	22	24.59	2.59	8.5	0.7
41	21.06	23.7	2.64	8.0	0.7
42	20	22.7	2.7	7.4	0.7
43	19	21.76	2.76	6.9	0.7
44	18	20.83	2.83	6.4	0.7
45	17	19.9	2.9	5.9	0.7
46	25	27.44	2.44	10.2	0.8
47	24	26.49	2.49	9.6	0.8
48	23	25.54	2.54	9.1	0.8
49	22	24.59	2.59	8.5	0.8
50	21.06	23.7	2.64	8.0	0.8
51	20	22.7	2.7	7.4	0.8
52	19	21.76	2.76	6.9	0.8
53	18	20.83	2.83	6.4	0.8
54	17	19.9	2.9	5.9	0.8
55	25	27.44	2.44	10.2	0.9
56	24	26.49	2.49	9.6	0.9
57	23	25.54	2.54	9.1	0.9
58	22	24.59	2.59	8.5	0.9
59	21.06	23.7	2.64	8.0	0.9
60	20	22.7	2.7	7.4	0.9
61	19	21.76	2.76	6.9	0.9
62	18	20.83	2.83	6.4	0.9
63	17	19.9	2.9	5.9	0.9
64	25	27.44	2.44	10.2	1.0
65	24	26.49	2.49	9.6	1.0
66	23	25.54	2.54	9.1	1.0
67	22	24.59	2.59	8.5	1.0
68	21.06	23.7	2.64	8.0	1.0
69	20	22.7	2.7	7.4	1.0
70	19	21.76	2.76	6.9	1.0
71	18	20.83	2.83	6.4	1.0
72	17	19.9	2.9	5.9	1.0
73	25	27.44	2.44	10.2	1.1
74	24	26.49	2.49	9.6	1.1
75	23	25.54	2.54	9.1	1.1
76	22	24.59	2.59	8.5	1.1
77	21.06	23.7	2.64	8.0	1.1
78	20	22.7	2.7	7.4	1.1
79	19	21.76	2.76	6.9	1.1
80	18	20.83	2.83	6.4	1.1
81	17	19.9	2.9	5.9	1.1
82	25	27.44	2.44	10.2	1.2
83	24	26.49	2.49	9.6	1.2
84	23	25.54	2.54	9.1	1.2
85	22	24.59	2.59	8.5	1.2
86	21.06	23.7	2.64	8.0	1.2
87	20	22.7	2.7	7.4	1.2
88	19	21.76	2.76	6.9	1.2
89	18	20.83	2.83	6.4	1.2
90	17	19.9	2.9	5.9	1.2
91	25	27.44	2.44	10.2	1.3
92	24	26.49	2.49	9.6	1.3
93	23	25.54	2.54	9.1	1.3
94	22	24.59	2.59	8.5	1.3
95	21.06	23.7	2.64	8.0	1.3
96	20	22.7	2.7	7.4	1.3
97	19	21.76	2.76	6.9	1.3
98	18	20.83	2.83	6.4	1.3
99	17	19.9	2.9	5.9	1.3
100	25	27.44	2.44	10.2	1.4
101	24	26.49	2.49	9.6	1.4
102	23	25.54	2.54	9.1	1.4
103	22	24.59	2.59	8.5	1.4
104	21.06	23.7	2.64	8.0	1.4
105	20	22.7	2.7	7.4	1.4
106	19	21.76	2.76	6.9	1.4
107	18	20.83	2.83	6.4	1.4
108	17	19.9	2.9	5.9	1.4
109	25	27.44	2.44	10.2	1.5
110	24	26.49	2.49	9.6	1.5
111	23	25.54	2.54	9.1	1.5
112	22	24.59	2.59	8.5	1.5
113	21.06	23.7	2.64	8.0	1.5
114	20	22.7	2.7	7.4	1.5
115	19	21.76	2.76	6.9	1.5
116	18	20.83	2.83	6.4	1.5
117	17	19.9	2.9	5.9	1.5